Feasibility Study on Visualized Ion Thruster

IEPC-2007-043

Presented at the 30th International Electric Propulsion Conference, Florence, Italy
September 17-20, 2007

Yoshinori Nakayama * and Yasuhiro Teraura †
National Defense Academy of Japan, Yokosuka, Kanagawa, 239-8686, Japan

Abstract: In order to contribute the inspections of numerical model for precise numerical analysis code development and the fundamental/educational understanding of ion thruster mechanism and ion beam optics behavior, a two-dimensional visualized ion thruster was designed and fabricated. Judging from the operations, probe measurements and spectroscopy measurements, it was cleared that this thruster can experimental visualize the schematic of ion production and extraction as described in conventional textbooks, that the ion beam extraction influences the ion density distribution in most of the discharge chamber, and that there is a close correlation between the ion beam focus position and the appropriate beam optics. These suggest that more detailed simulation of wide-ranging plasma discharge and sheath is necessary for a durability evaluation code development.

I. Introduction

In these days, many ion thrusters are installed in various types of satellites; geostationary orbit satellites, space probes and so on. Since the ion thrusters are getting recognitions as space propulsion systems through the actual uses in space, it is expected to increase the installation numbers and the types. A durable ion thruster with operatable time of over a few years is to be one of attractive thrusters in near future. This is because the long durability thruster is useful for a deep space probe and a long-operated satellite. The development of the long durability thruster needs a precise numerical analysis for the confirmation of its durability, because the experimental confirmation needs high cost and long time. Many numerical analyses have been studied for the design-aid of ion thrusters. Nevertheless, the numerical analysis codes have been not completed. It is considered that the reason includes the difficulty of numerical model inspection compared with the experiments. We considered that a two-dimensional ion thruster was to contribute the inspections, that is, the development of the precise numerical analysis code. In addition, we also considered that a visualization of ion thruster was to contribute the inspections by other method; a noncontact optical measurement.

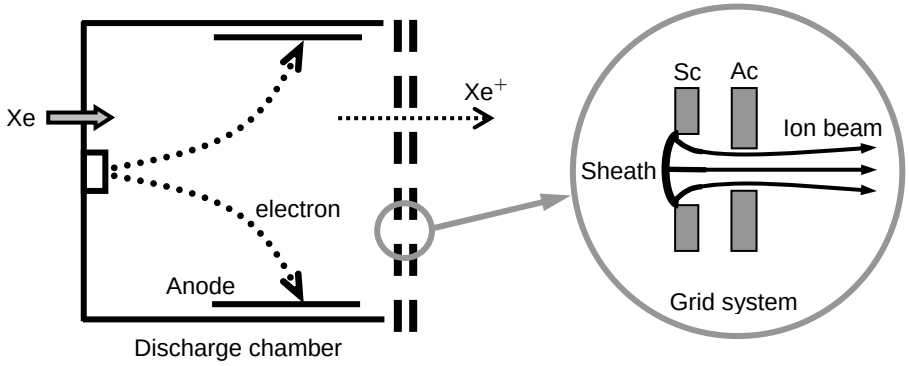

Figure 1. Schmatic of ion thruster discharge chamber and grid system.

* Associate Professor, Department of Aerospace Engineering, ynakayam@nda.ac.jp.
† Master's Degree Student, Department of Aerospace Engineering, g45026 @nda.ac.jp.

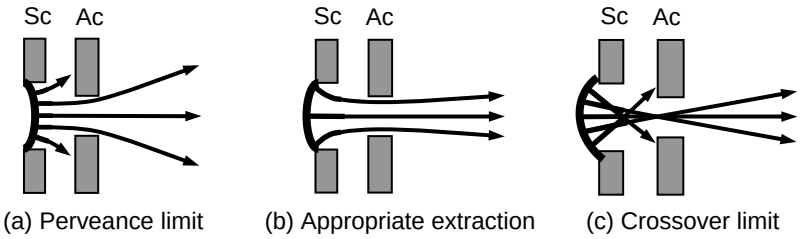

Figure 2. Schmatic of ion beam focusing.

The purposes of this study are (1) design and fabrication of the visualized ion thruster (VIT), and (2) evaluation of the thruster. Since this thruster materialized the well-known two-dimensional schematic of ion thruster as shown in Fig. 1, it seems that this VIT can also contribute the fundamental/educational understanding of ion thruster mechanism and ion beam optics behavior as shown in Fig. 2.[1-3]

II. Thruster Design

A. Ion Source

The shape of VIT is two-dimensional rectangular parallelepiped as shown in figure 3. The plasma is produced by direct current discharge, that is, the VIT is an electron bombardment type thruster. The discharge chamber wall is composed of a pair of L-shape iron yokes, a pair of rectangle glass plates and a rectangle stainless steel grid system. The dimensions of the discharge chamber are 80 x 50 x 80 mm. The yokes are set for the magnetic field formation, and the glass plates are set for the spectroscopy measurement. Within the discharge chamber, three pairs of rectangle stainless steel anodes are set. Changing the electrical connection to the one of anodes or all anodes is intended to switch the discharge path. There is an electron source at the center of the upstream discharge chamber wall. The electron is produced by a filament within the source, and is emitted to the discharge chamber through the keeper bridge plasma. The xenon propellant particle flows into the chamber through the electron source, is ionized by the electron bombardment, and is extracted by the grid system.

B. Grid System

The grid system of VIT is composed of two or three rectangle stainless steel grids. The each grid has three narrow slits in y-direction. In this study, this grid system has a screen grid and a acceleration grid. The thickness, slit

Figure 3. VIT photograph

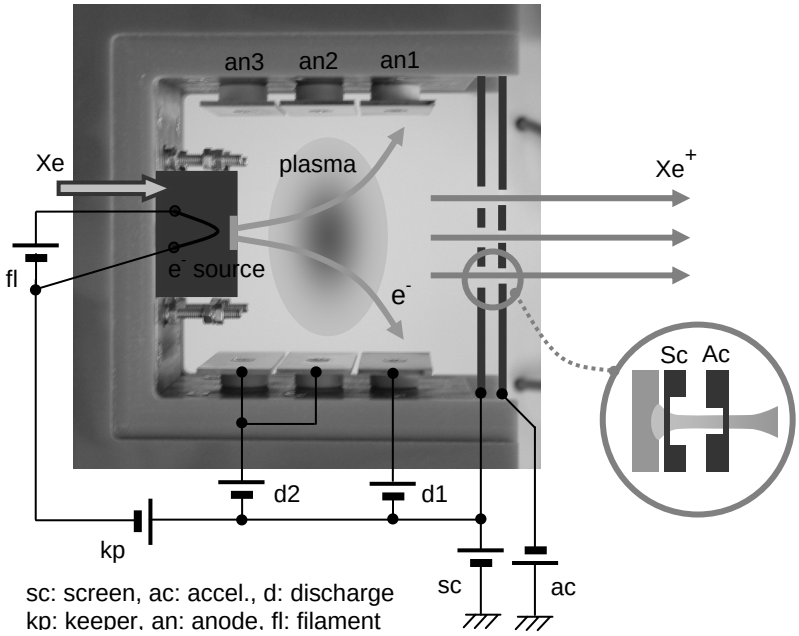

Figure 4. Schematic of VIT and its electric circuit.

pitch and slit length of both grids are 1.5 mm, 5.0 mm and 30 mm, respectively. The slit widths of the screen and acceleration grid are 3.0 mm and 2.0 mm, respectively. The screen grid is fixed to the discharge chamber, and the acceleration grid is fitted to the discharge chamber with four stainless steel springs and four ceramics screws to keep a gap of 0.8 mm. The slits of viewer's side (in +y-direction) was canaliform machined as shown in Fig. 4 in order to observe most of ion beam optics. The remained thickness is 0.2 mm. Since the slit grid system extracts three sheet-shaped ion beams, a viewer can observe three bright ion beams if the viewer see them from +y-direction.

III. Experimental Procedure and Apparatus

A. VIT Operation

A schematic of the electric circuit for this experiment is shown in Fig. 4. The screen grid is connected electrically to the discharge chamber. In this study, all anode potential is the same. The VIT is operated at the following condition: the propellant flow rate of 0.60 sccm (60 micro-g/s, Xe), the discharge voltage of 50 V, the total discharge current of 0.45 A, the keeper current of 0.10 A. The keeper voltage is 40 V at off-discharge condition, and the voltage instantly decrease to approximately 0 V due to the constant current control at on-discharge condition. The screen grid potential is 0-2 kV, and the acceleration grid potential is -200 V. These currents and potentials are applied with their errors of 1%. The error of propellant flow rate control is below approximately 1%. The vacuum pressure was approximately 3 mPa when the xenon flow rate was 0.60 sccm. After the VIT operating condition is stable, the following probe and spectroscopy measurements are performed. The probe measurement is only performed for the evaluation of produced plasma uniformity.

B. Measurement Points and Areas

Figure 5 shows the schematic of the measurement points and areas. The small circles indicate the probe measurement locations in x-z direction. The bold regular tetragons indicate the spectroscopy measurement areas. The areas are in a reticular pattern with a lattice spacing of 10 mm in both x-direction and z-direction. These locations is named with three letters. The second letter with x-direction location equivalent and the third letter with z-direction location equivalent are followed after the first letter "p." For example, the original point in this figure is named "p00." The p06 point coincides with the center of grid system.

C. Probe Measurements

A 0.20 mm diameter pure tungsten wire that is almost covered with a 1.0 mm diameter ceramics tube is used as a langmuir probe. The exposed length is 0.08 mm. This prove is inserted to the discharge chamber through a small hole of a glass plate, and is moved in y-direction in order to undisturb the plasma production. The locations in y-direction are y=0.0, +7.5, +15.0 and +22.5 mm. The location error is below 1 mm in all directions. The reference potential of this probe is as high as the discharge chamber wall potential, that is, the screen grid potential. The probe potential of 0-100 V is applied, and the probe current is measured with a noncontact inductive ammeter. The probe measurements are performed under non-extraction condition.

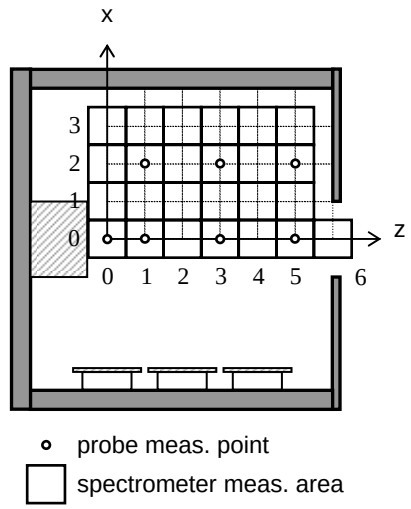

Figure 5. Measurement points and areas

D. Spectroscopy Measurements

In order to divide the measurement area, a lattice made of 29 square pipes is arranged between the VIT glass plate and a glass porthole of vacuum chamber, with little clearance. The location error is below 0.5 mm in both directions. The divided light is detected by a spectrometer via a fiber-optic cable. In order to correct the spectroscopy intensity of each area, a spatially-uniform light, a LCD for PC, was detected as the reference in preliminary experiment. All measured spectroscopy intensity is compensated with the correction factor derived from this preliminary experiment.

IV. Results and Discussion

A. Experimental Visualization

Figure 6 shows the discharge plasma and three ion beams that were directly observed through the VIT glass plate. The slightly

bright line at the right of grid system is the plasma light reflected by the glass plate edge. As will hereinafter be described in detail, the plasma sheath near the grid system was also clearly observed. It seems that the VIT can experimental visualize the schematic of ion production and extraction as shown in figure 1.

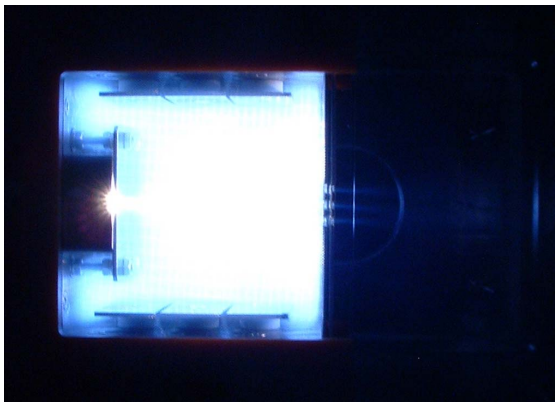

Figure 6. VIT in operation

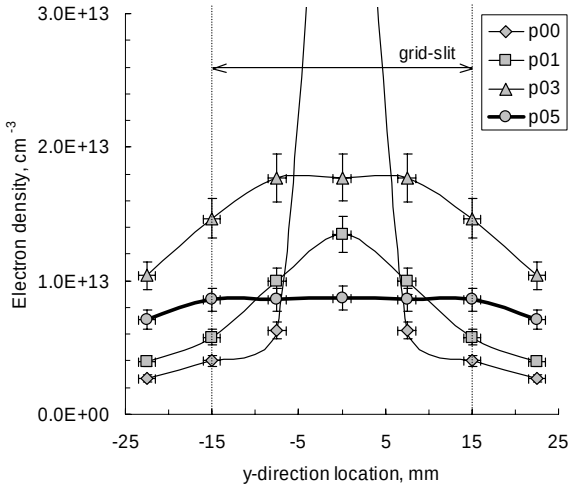

Figure 7. Plasma uniformity in center area

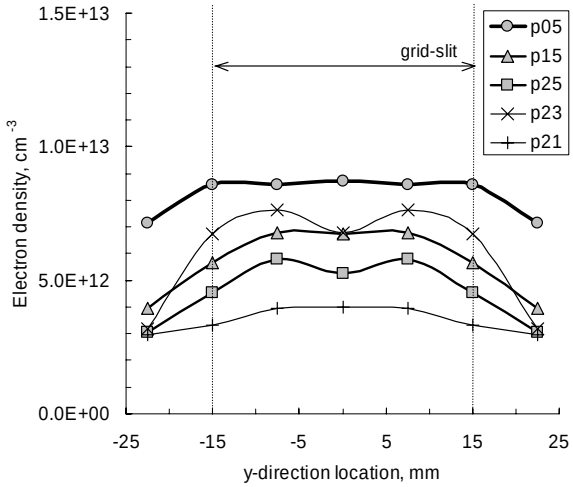

Figure 8. Plasma uniformity in outlying area

B. Plasma Uniformity

The distributions of electron number density within the discharge plasma are shown in Figs. 7 and 8. The reproducibility error ratio is approximately 5% at most of measurement points. As shown in Fig. 7, the density at the p00 and p01 point is not uniform in y-direction. This is because these points are near the keeper plasma emission hole. The density at p00 (y=0.0 mm) was approximately 5.4×10^{13} cm^{-3}. The density at the outside of keeper plasma is relatively uniform in y-direction. The density at near the grid system, p05, is almost perfectly uniform in y-direction, especially. The electron number density and electron temperature are approximately 8.4×10^{12} cm^{-3} and 3 eV, respectively. These values differ little from those of the conventional dc ion thrusters. The plasma space potential in this uniformly region is 52-54 V that is 2-4 V higher than the anode potential.

C. Luminescence Intensity

Figure 9 indicates the luminescence intensity measured by the spectrometer against the electron number density measured by the probe. The reproducibility error ratio is approximately 5%. The 467 nm and 823 nm are the typical luminescence wavelength of xenon ion and neutral, respectively. Both intensities are almost proportional to the density. Under the non-extraction condition, it was cleared that the ratio of 467 nm intensity to 823 nm intensity is almost constant.

D. Ion Extraction

Figures 10 and 11 indicate the luminescence intensity distributions under non-extraction (in the upper half) and

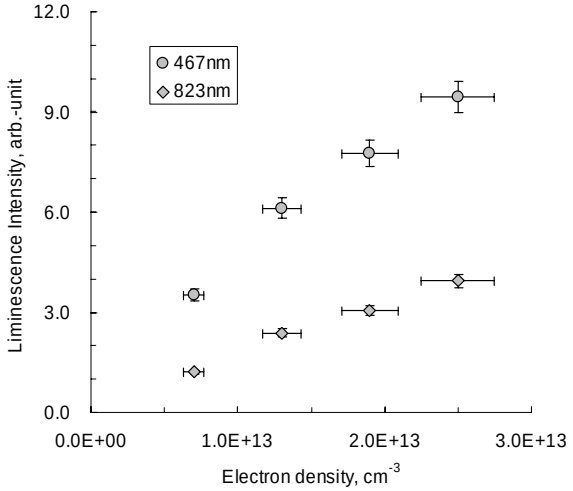

Figure 9. Ion, neutral and electron density

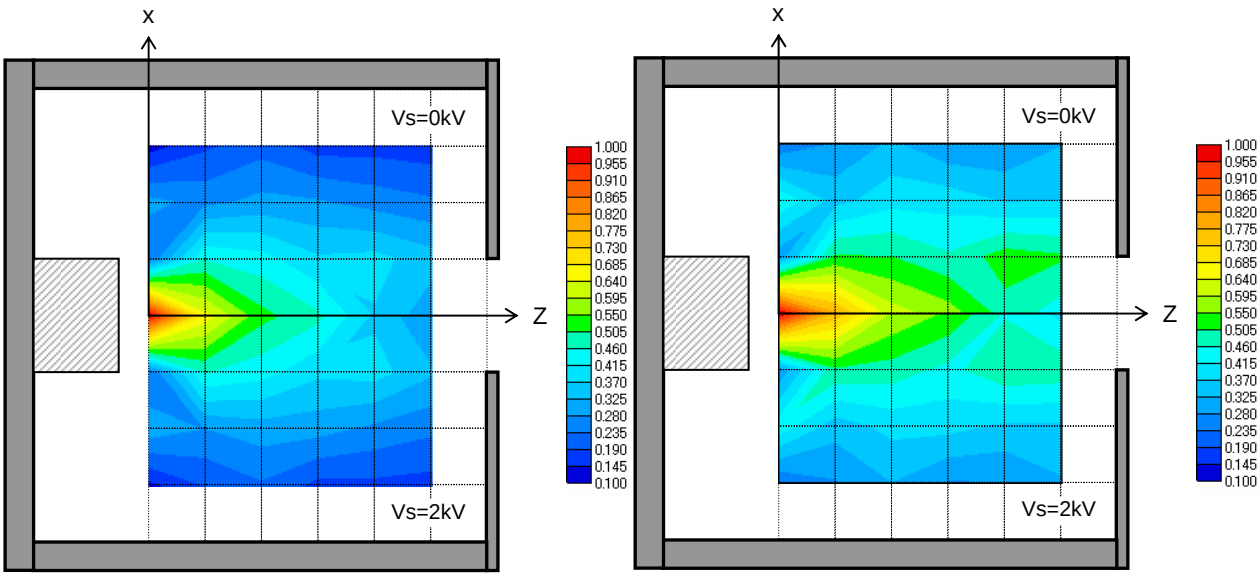

Figure 10. Neutral density ratio

Figure 11. Ion density ratio

extraction condition (in the lower half). In both figures, the intensity at the original point (p00) is 1.0 as the reference value. Since the produced plasma uniformity and the proportional relationship between the luminescence intensity and the electron number density were confirmed, it seems that these distribution ratios are equivalent to those of xenon neutral and ion density. These figures indicate that the ion extraction influences the ion density within the discharge chamber, on the other hand, little influences the neutral density. This is because the electric field does not act the neutral particle.

Figure 12 indicates the ratio of ion luminescence intensity when ions were extracted by 1 kV (in the upper half) and 2 kV (in the lower half) screen grid potential, to that when ions were not extracted. This figure suggests that an ion beam extraction influences an ion density distribution in most of discharge chamber, not only near a grid system. Therefore, it is necessary that the more precise numerical analysis of ion beam extraction can simulate the wide-ranging influences of ion density distribution or plasma production in the discharge chamber.

Figure 13 shows the photographs of the plasma near the grid system in some screen grid potential cases. The plasma sheath profile near the grid slit becomes convex when the screen grid potential was set at 0 kV, on the other hand, the sheath profiles become concave when the screen grid potential was set at 1 kV and 2 kV. It seems that the VIT can experimental visualize the schematic of ion extraction as shown in Fig. 2. In addition, the number of observed bright lines in the plasma is three in the non-extraction case, and it is four in the extraction cases. The more detailed study is to be necessary for the identification of these lines.

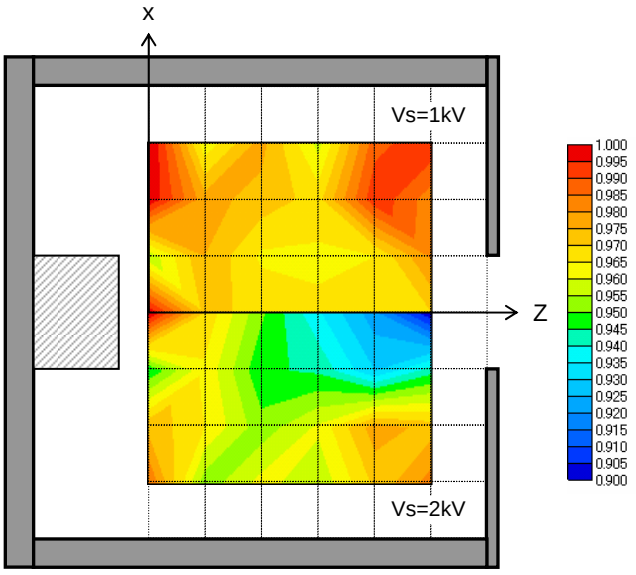

Figure 12. Decrease ratio of ion density

Figure 14 shows the photographs of the plasma sheath and ion beam in some screen grid potential cases. The ion beam impinged to the acceleration grid when the screen grid potential was set over 1.25 kV. This phenomenon agrees well with the change of acceleration grid current against the screen grid potential as shown in Fig. 15. In addition, as the screen grid potential is higher, the concave sheath is larger, and the beamlet focus position is toward the screen grid from the acceleration grid on the center axis. Figure 16 indicates the position of the focus position (Z_f) and the sheath edge position on the center axis (Z_s) against the screen grid potential. These position are the distance from the center of screen grid upstream surface. The sheath edge points were roughly determined from the low-graded high-

contrasted photographs. Figure 17 indicates the distance between the focus point and the sheath edge point (Z_f-Z_s) against the screen grid potential with the change of the acceleration grid drain current ratio. Figure 18, redrawn with these figures, was the screen grid potential and the acceleration grid drain current ratio against the beamlet focus position. Figure 19 indicates the minus three-halves power of the net acceleration potential (V_n) against the beamlet focus position. These figures suggest that (1) both the focus position and the sheath edge position are moving upstream as the screen grid potential is higher, (2) the distance between the focus point and the sheath edge point is almost constant when the ion beam impinged to the acceleration grid, (3) the ion beam impinges to the acceleration grid when the beamlet focus position is in the gap between the screen and acceleration grid, and (4) the beamlet focus position is proportional to the minus three-halves power of the net acceleration potential. Although it is necessary to investigate if these phenomena are general or particular in this grid system, it is convenient to think that the close correlation between the positions and the appropriate beam optics was confirmed.

V. Conclusion

Through probe and spectroscopy measurements of a two-dimensional visualized ion thruster operation, it seems that the comparative evaluation between the experimental data and a simulated results, the plasma sheath profiles and ion beam focus position, is to contribute the development of numerical analysis code which can precisely simulate an ion thruster durability. In addition, this thruster that experimental visualize a well-known schematic described in some conventional textbooks is to be also useful for the fundamental/educational understanding of ion thruster mechanism and ion beam optics behavior.

References

[1]Jahn, R. G., *Physics of Electric Propulsion*, 1st ed., McGraw-Hill, New York, 1968, Chap. 7.

[2]Stuhlinger, E., *Ion Propulsion for Space Flight*, McGraw-Hill, New York, 1964, Chap. 5.

[3]Lieberman, M. A., *Principle of Plasma Discharges and Materials Processing*, John Wiley & Sons, New York, 1994, Chap. 6.

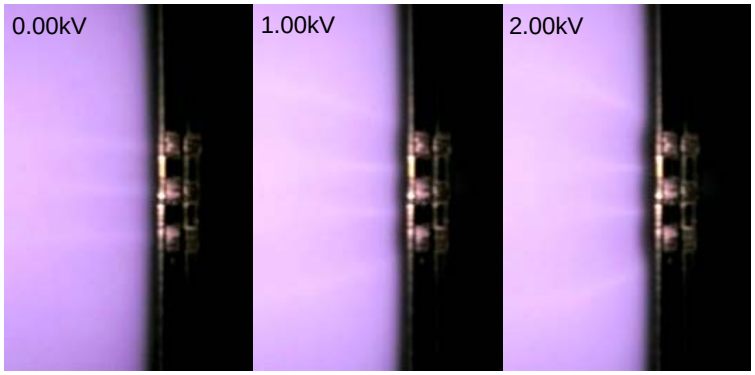

Figure 13. Plasma sheath profiles

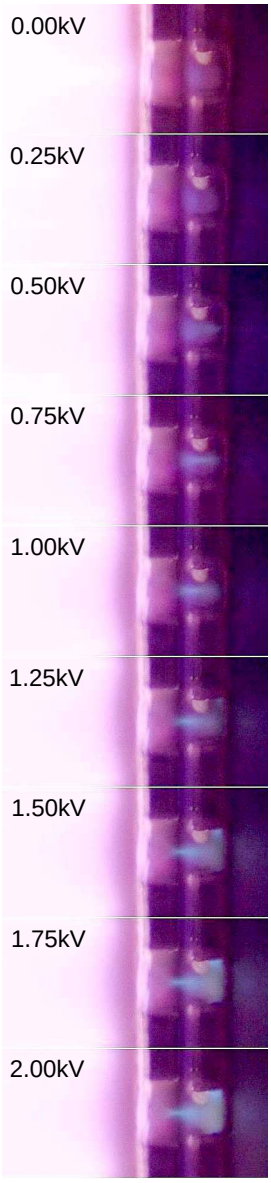

Figure 14. Ion beams

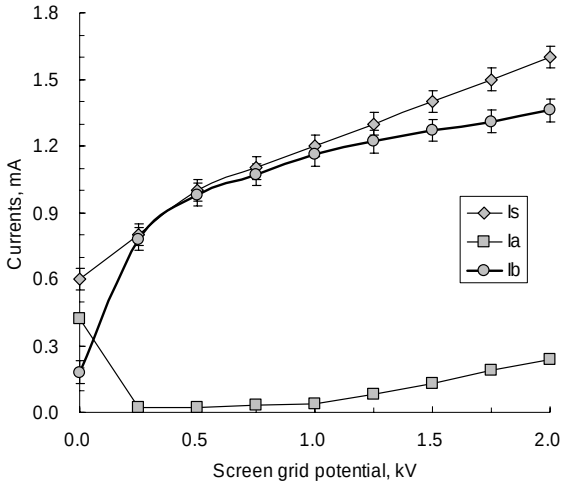

Figure 15. Grid currents (three slits)

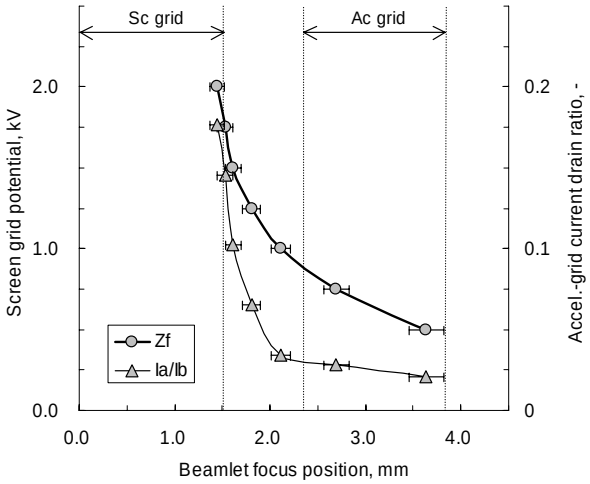

Figure 18. Focus position and drain ratio

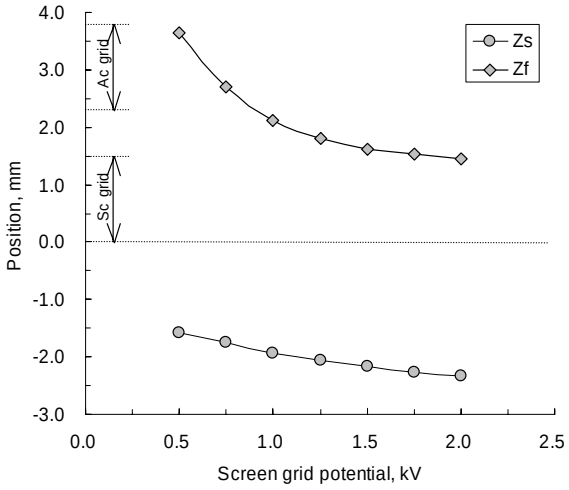

Figure 16. Position of sheath edge and focus

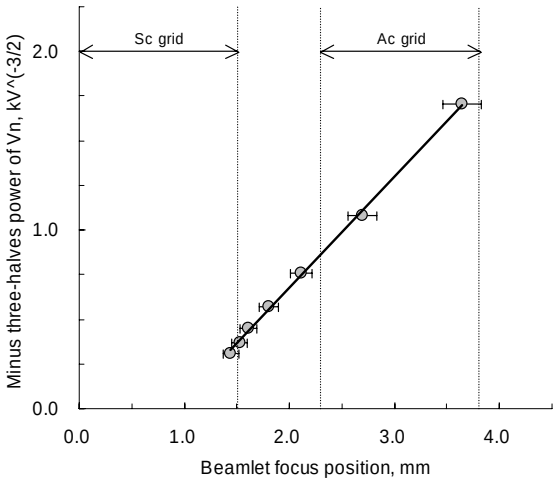

Figure 19. Focus position and $V_n^{-2/3}$

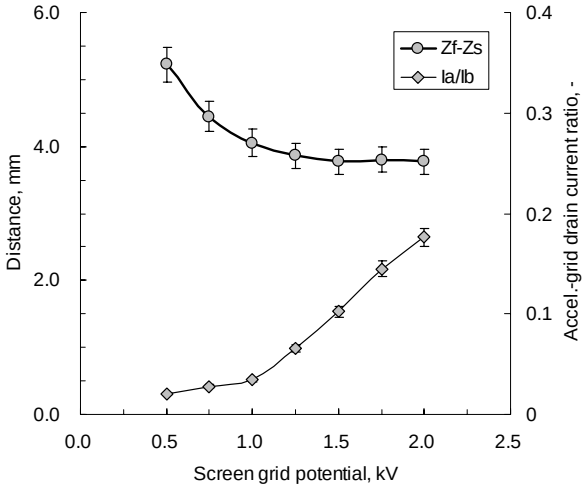

Figure 17. Distance between Z_s and Z_f